Scanning Microscopy Vol. 11, 1997 (Pages 379-390) 0891-7035/97$5.00+.25
Scanning Microscopy International, Chicago (AMF O'Hare), IL 60666 USA

MAXIMUM ENTROPY RESTORATION OF ELECTRON MICROSCOPE IMAGES WITH A RANDOM-SPATIAL-DISTRIBUTION CONSTRAINT

T. Hanai[1]*, T. Morinaga[1], H. Suzuki[1] and M. Hibino[2]

[1]Department of Electronics, School of Engineering, [2]Center for Integrated Research in Science and Engineering, Nagoya University, Nagoya, 464-01 Japan

Abstract

An improved maximum entropy (ME) method is proposed for restoration of electron microscope images of extended objects for which the conventional ME method has not presented satisfactorily restored images. For the improvement of ME restoration, a constraint consistent with statistical properties of quantum noise contained in observed images was introduced to impose a random spatial distribution (RSD), in addition to a suitable probability distribution, on the inferred noise.

The ME restorations with and without the RSD constraint were applied to models of scanning transmission electron microscopy (STEM) images degraded by a Gaussian point spread function and a Poisson noise. The RSD constrained ME method recovered both point and disk objects by suppressing the localization of the large noise into the object sites. The signal-to-noise ratio of the restored image of disk objects was higher for the ME restoration with the RSD constraint than the original degraded image and the restoration without the RSD constraint. The ME restoration was also applied to models of largely defocused noisy transmission electron microscopy (TEM) images of weak phase objects. For point objects, the ME restoration with the RSD constraint as well as the conventional ME restoration using χ^2 constraint improved the resolution. For disk objects, only the RSD constrained ME restoration successfully removed fringes due to the defocus and decreased quantum noise.

Key Words: Image restoration, maximum entropy method, electron microscopy, scanning transmission electron microscopy, quantum noise.

*Address for correspondence:
Takaaki Hanai
Department of Electronics, School of Engineering
Nagoya University
Nagoya, 464-01 Japan
Telephone number: +81 (52) 789 4438
FAX number: +81 (52) 789 3155
E-mail: hanai@nuee.nagoya-u.ac.jp

Introduction

The Maximum Entropy (ME) method has been successfully used in various fields for restoration of blurred noisy images (Gull and Skilling, 1984; Narayan and Nityananda, 1986). In electron microscopy, the ME method has been applied to deconvolution of atomic-scale dark-field scanning transmission electron microscope (STEM) images (Pennycook *et al*., 1994), and deconvolution of transmission electron microscope (TEM) images with unknown defocus amount (Hu and Li, 1991).

However, the ME restoration failed to improve the signal-to-noise ratio (SNR) when it was applied to STEM images of extended objects with considerably large areas (Farrow and Ottensmeyer, 1989). The reason for the failure of the restoration was that maximization of the entropy required smooth intensity distributions and, therefore, decreased image contrasts. For this smoothing of the processed image, the inferred noise having large magnitudes was assigned to the extended object region. This localization of the inferred noise is not consistent with the statistical property of quantum noise because the spatial distribution of the amplitude of quantum noise is random. Satisfactory restoration is not obtained if the inferred noise largely deviates from the actual noise in each pixel. Therefore, it is expected that introduction of a statistical constraint imposing a random spatial distribution of the inferred noise allows better restoration for images of extended objects. Farrow and Ottensmeyer (1989) proposed application of simulated annealing method to realize the random spatial distribution of the noise. This method seems to be useful for stochastic problems such as the ME restoration but a disadvantage of a long computation time should be overcome for images with a large number of pixels.

We propose a simple method to realize the random spatial distribution (RSD) of the noise by fitting, in the reciprocal space, the power spectrum of inferred noise residuals to the uniform power spectrum of the spatially random noise (Hanai *et al*., 1994). In addition to the RSD constraint, exact error fitting constraint (E constraint) (Bryan and Skilling, 1980) was used to fit the probability density of the noise amplitude to the statistical expectation. This two-fold constraint, which restricts both probability distribution

and spatial distribution of the inferred noise amplitude, is denoted as the *E+RSD* constraint below. In this paper, the ME method with the E+RSD constraint is described in detail. Results of simulations using models of STEM and TEM images are shown for point objects and extended objects, and compared with the results of conventional χ^2 constrained ME restoration. Simulations for noisy low resolution images, for which the E+RSD constrained ME restoration would be most useful, are mainly dealt with in this paper and the case of high resolution image is described briefly.

Methods

In the ME method, an image is restored by maximizing the entropy of the image under constraints which are consistent with the observed image and statistical properties of the noise. There are several formulas for definition of the entropy and their difference has been discussed (Kikuchi and Soffer, 1977; Frieden, 1983). In this paper we adopt the entropy form

$$S = -\sum_{j=1}^{N} f_j [\log (f_j / A) - 1] \tag{1}$$

Skilling and Bryan, 1984) for reason of computational efficiency. In Equation (1), f_j denotes the number of electrons in jth pixel of the ideal image without blurring and noise, A the average of f_j over the image and N the number of pixels. Here, the image is represented by a vector in a N dimensional space as $\boldsymbol{f} = (f_1, f_2, \cdots, f_N)$. The general aim of image restoration techniques is to find the most probable $\boldsymbol{f}$ from an observed image $\boldsymbol{D} = (D_1, D_2, \cdots, D_N)$ or a series of observed images. When the observed image is corrupted by noise, there are many probable images on different bases. Among all probable images, the maximum entropy image carries minimum information because the entropy is the measure of uncertainty. It means that the maximum entropy image contains minimum structure which is consistent with the observed image. This is the reason why the ME restoration is considered to have the least artefacts. Practically, the ME restoration has a merit of providing smooth intensity distribution to maximize the entropy if no confidential structure is recognized in the observed image.

The number of electrons falling in kth pixel of the observed image is written as

$$D_k = F_k + n_k \sigma_k \tag{2}$$

where σ_k denotes the standard deviation of the noise, n_k a random variable which represents the normalized noise residual and F_k the number of electrons in the image which would be obtained in the absence of noise. In a linear and space-invariant imaging, $\boldsymbol{F} = (F_1, F_2, \cdots, F_N)$ is given by the convolution of $\boldsymbol{f}$ with a point spread function $\boldsymbol{R}$ and is expressed using the matrix form of $\boldsymbol{R}$ as

$$F_k = \sum_{j=1}^{N} R_{kj} f_j \tag{3}$$

The ME restoration selects the single solution for $\boldsymbol{f}$ with the maximum entropy from possible images for which the series of the residuals $\boldsymbol{n} = (n_1, n_2, \cdots, n_N)$ calculated from Equation (2) satisfies statistical constraints.

The conventional ME restoration uses a χ^2 constraint in which a statistic

$$\chi^2 = \sum_k (F_k - D_k)^2 / \sigma_k^2 = \sum_k n_k^2 \tag{4}$$

is restricted to reasonable values around the statistical expectation. When quantum noise is dominant, the electron number fluctuates according to the Poisson distribution, so that

$$\sigma_k = \sqrt{F_k} \tag{5}$$

and n_k follows the normal probability distribution $N(0, 1)$ if the number of electrons is well above unity in each pixel.

An alternative constraint has been proposed (Bryan and Skilling, 1980) as E constraint which minimizes the distance between the probability distribution of the residuals n_k and the normal distribution. In the process of the E constrained ME restoration, residuals n_k are sorted into ascending order to give $n_{(i)}$ ($n_{(1)} < n_{(2)} < \cdots < n_{(N)}$), and a statistic

$$E = \{\sum_{i=1}^{N} (n_{(i)} - v_{(i)})^2\}^{1/2} \tag{6}$$

is minimized, where $v_{(i)}$ is the ith element of the numerical series sampled from a population obeying the normal distribution and sorted into ascending order. The ME restoration is reduced to a constrained maximization of the entropy S which can be solved by maximizing a Lagrangian function

$$Q = S - \lambda E \tag{7}$$

in the case of the E constraint, where λ is the Lagrange multiplier and E is calculated with Equation (6). Although the E constraint has a mathematically weak basis so that the solution may not be unique, we employed this constraint because of its practical merit of giving better deconvolution effect. The E constraint provides a strict fitting of the probability of the noise amplitudes but still assigns biased residuals to the noise at the object sites and decreases the image contrast for extended objects. Therefore, the

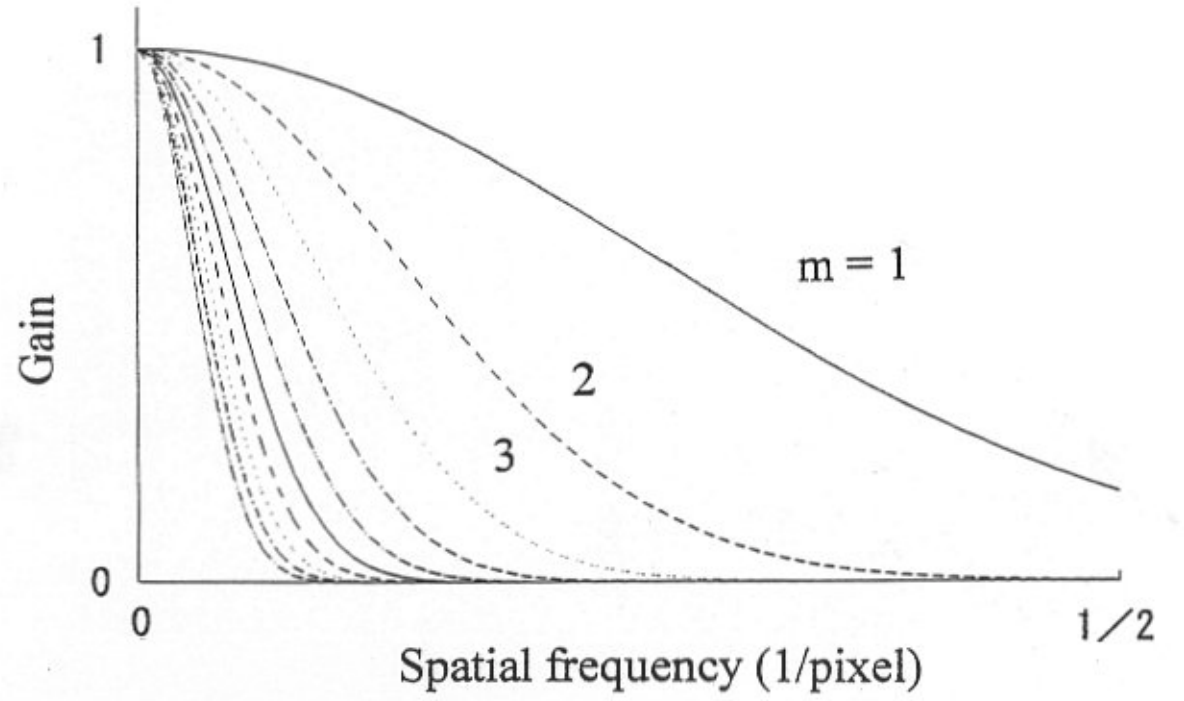

Figure 1. Low-pass filters used to divide the spatial frequency domain into several frequency bands in which the power spectrum of the inferred noise was integrated to evaluate its flatness. The half width of the filter is in proportion to the inverse of *m*.

performance of ME restoration is considered to be improved if the undesirable concentration of the noise is avoided.

We propose a new method to realize a random spatial distribution of the inferred noise. The method uses a property of quantum noise having a uniform power spectrum in the spatial frequency domain and minimizes the deviation of the power spectrum of inferred noise residuals from the uniform power spectrum. In order to perform this minimization in a reasonable computation time, the spatial frequency domain is divided into several frequency bands using low-pass filters with different band widths. Both the power spectrum of the inferred residuals and the expected uniform power spectrum are low-pass filtered and integrated to give the total powers contained in these frequency bands, and the differences of the powers are minimized simultaneously in all frequency bands. The low-pass filters used in the present work are Gaussian functions as shown in Figure 1 although other filter forms might be also applicable. The *m*th low-pass filter in Figure 1 has a full width at half maximum (FWHM) in proportion to 1/*m*. This RSD constraint was combined with the maximization of the E constrained entropy function given by Equation (7). We call this process E+RSD constrained ME restoration. The algorithm for the constrained maximization basically follows Skilling's proposal (Skilling and Bryan, 1984) and the new constraint on the power spectrum is incorporated in the algorithm as detailed below.

Once an trial image for $\boldsymbol{f}$ without blurring and noise is assumed, the residuals $\boldsymbol{n} = (n_1, n_2, \cdots, n_N)$ are determined from Equation (2). Let the residuals passed by the *m*th low-pass filter be $\boldsymbol{n}^{(m)} = (n_1^{(m)}, n_2^{(m)}, \cdots, n_N^{(m)})$ Then, $\boldsymbol{n}^{(m)}$ is written with the convolution formula as

$$n_k^{(m)} = \sum_{j=1}^{N} R_{kj}^{(m)} n_j \tag{8}$$

where the convolution matrix $\mathbf{R}^{(m)}$ is derived from the inverse Fourier transform of the low-pass filter. From the Parseval's theorem, the integral of the power spectrum for $\mathbf{n}^{(m)}$ is identical to the power calculated in real space as

$$B_m(\mathrm{n}) = \sum_{\mathrm{k}=1}^{\mathrm{N}} (\mathrm{n}_{\mathrm{k}}^{(\mathrm{m})})^2 \tag{9}$$

For simplicity, it is supposed that only two low-pass filters are used for fitting of the power spectrum of the residuals. Then, three values of the integrated power $B_1(\boldsymbol{n})$, $B_2(\boldsymbol{n})$ and $B_3(\boldsymbol{n})$ are obtained from different spatial frequency domains. One is the total power integrated over the whole frequency range and the others are the powers passed by the two filters. To minimize the differences of these powers from their expectations $B_{1\mathrm{aim}}$, $B_{2\mathrm{aim}}$, and $B_{3\mathrm{aim}}$, respectively, the gradients of $B_m(\boldsymbol{n})$ (m = 1, 2, 3) in the N dimensional

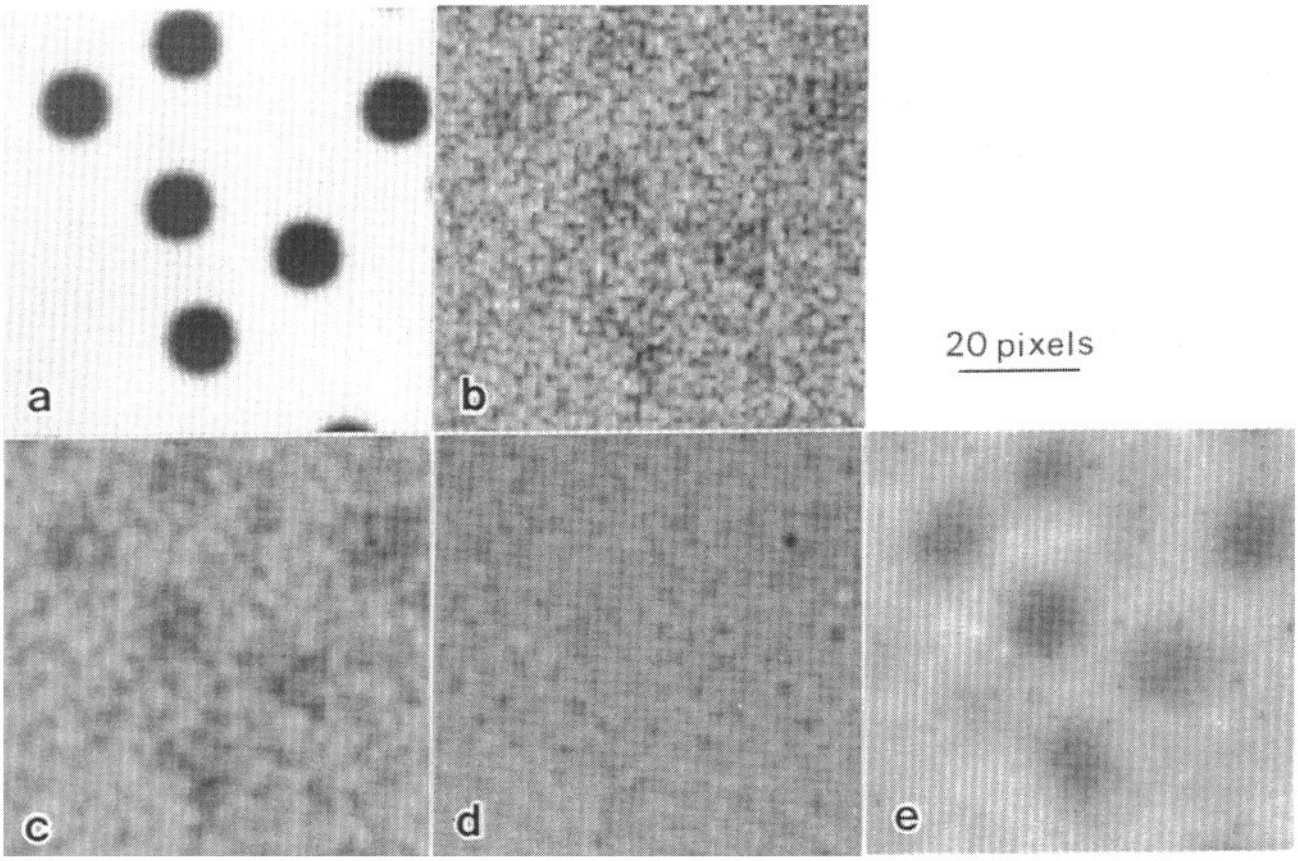

Figure 2. A model of the bright-field STEM image of disk objects and restored images. The image (**a**) shows disks of 6 pixels in radius convoluted with a Gaussian point spread function of the FWHM of 2 pixels, (**b**) corrupted by the random noise simulating a Poisson distribution of the number of electrons. Images (**c**), (**d**) and (**e**) are results of restorations with the χ^2, independent E and E+RSD constraints, respectively.

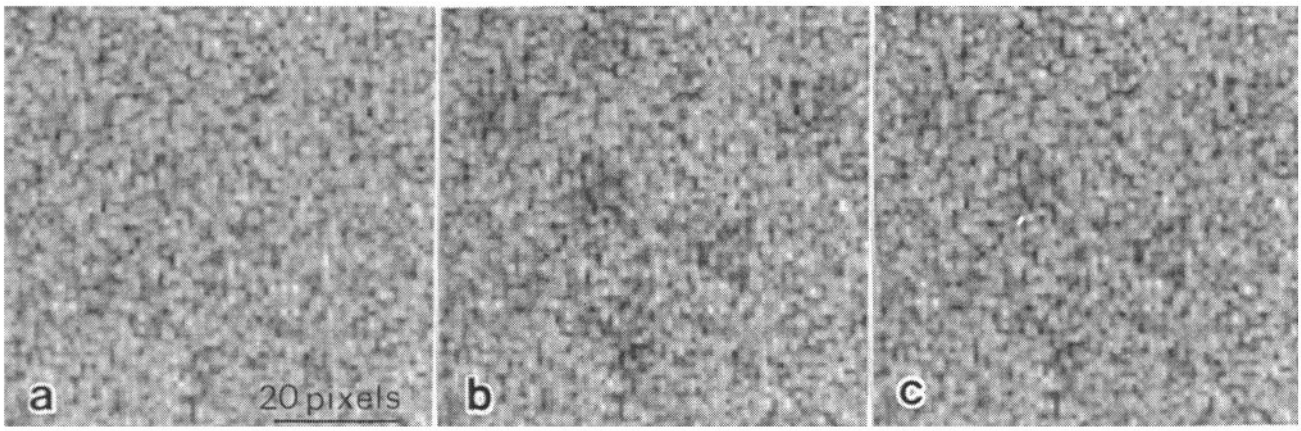

Figure 3. Maps of the residuals calculated from the observed and restored images shown in Figure 2. The map (**a**) shows the original random noise. The maps (**b**) and (**c**) show the residuals inferred by the χ^2 and E+RSD constrained ME restorations.

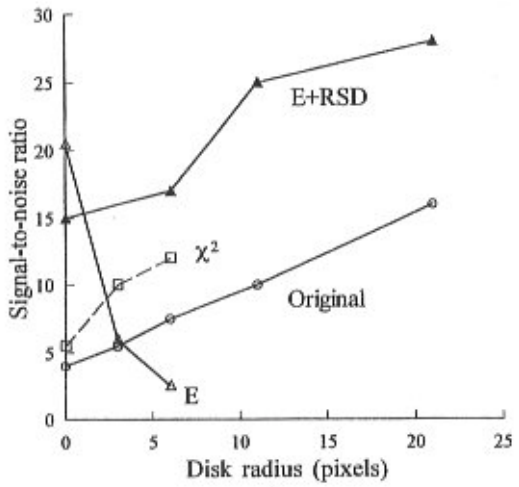

Figure 4. Signal-to-noise ratio, after Rose's criterion, of the original degraded images and restored images for various size of objects. The radius of zero pixel indicates point objects.

space are calculated as

$$\nabla B_m = \left(\frac{\partial B_m}{\partial n_1}, \frac{\partial B_m}{\partial n_2}, \ldots, \frac{\partial B_m}{\partial n_N}\right) \tag{10}$$

Since the differentiation $\partial B_m/\partial n_l$ is derived from Equations (8) and (9) as

$$\frac{\partial B_m}{\partial n_l} = \sum_{k=1}^{N} \frac{\partial B_m}{\partial n_k^{(m)}} \frac{\partial n_k^{(m)}}{\partial n_l} = 2\sum_{k=1}^{N} n_k^{(m)} R_{kl}^{(m)} = 2\sum_{k=1}^{N}\sum_{j=1}^{N} R_{kl}^{(m)} R_{kj}^{(m)} n_j \tag{11}$$

Equation (11) involves the two-fold convolution of $\boldsymbol{n}$ with the symmetric matrix (corresponding to the two-fold low-pass filtering of $\boldsymbol{n}$) which can be readily calculated with fast Fourier transform.

The next step is to search for the position, where B_1, B_2 and B_3 are approximately equal to B_{1aim}, B_{2aim} and B_{3aim}, respectively, in a space subtended by base vectors $\boldsymbol{e}_1 = \nabla B_1$, $\boldsymbol{e}_2 = \nabla B_2$ and $\boldsymbol{e}_3 = \nabla B_3$. This space is a subspace of the N dimensional space used for representing images with N pixels, and the reduction of the dimension of the searched space largely reduces the computation time. To solve this problem, simple steepest descents method is used. In this method $B_m(\boldsymbol{n})$ is approximated by the first order Taylor expansion with respect to the displacement $\boldsymbol{x} = (x_1, x_2, x_3)$ in the subspace as

$$B_m(\boldsymbol{n}) = B_{m0} + b_{m1}x_1 + b_{m2}x_2 + b_{m3}x_3 \tag{12}$$

with

$$\boldsymbol{n} = \boldsymbol{n}_0 + x_1\boldsymbol{e}_1 + x_2\boldsymbol{e}_2 + x_3\boldsymbol{e}_3 \tag{13}$$

and

$$b_{mn} = \nabla B_m \cdot \boldsymbol{e}_n \tag{14}$$

where $\boldsymbol{n}_0$ is the noise residuals inferred in the previous iteration of the loop in the ME restoration program and B_{m0} is the integral of the low-pass filtered power spectrum for $\boldsymbol{n}_0$. The necessary displacement $\boldsymbol{x}$ can be obtained by solving linear equations

$$\begin{bmatrix} b_{11}b_{12}b_{13} \\ b_{21}b_{22}b_{23} \\ b_{31}b_{32}b_{33} \end{bmatrix} \begin{bmatrix} x_1 \\ x_2 \\ x_3 \end{bmatrix} = \begin{bmatrix} B_{1aim} - B_{10} \\ B_{2aim} - B_{20} \\ B_{3aim} - B_{30} \end{bmatrix} \tag{15}$$

The noise residuals $\boldsymbol{n}$ obtained from Equations (13) and (15) should have a more uniform power spectrum than $\boldsymbol{n}_0$ because the power of the noise is evenly assigned to the spatial frequency bands correspondingly to their band widths. With the modified $\boldsymbol{n}$, the value of the E statistic is calculated with Equation (6) and the maximization of Equation (7) is performed with Skilling's algorithm. This procedure is repeated until convergence. The computation time depends on the SNR of the processed image and, in most cases, the CPU time of a main frame computer used for process of a 128x128 pixel image is within 5-30 seconds for the χ^2 constraint and about five times longer for the E+RSD constraint.

Restoration of Models of STEM Images

The effect of ME restoration on STEM images was studied with model images. It was assumed that the imaging is completely incoherent, the intensity distribution of the electron probe is Gaussian with a known diameter and quantum noise is the dominant noise. The model images were, therefore, prepared by convoluting objects with the Gaussian point spread function and introducing random fluctuation of the electron number obeying a Poisson distribution. An example of blurred bright-field STEM image of disk objects is shown in Figure 2a. The radius of the objects is 6 pixels and the FWHM of the point spread function is 2 pixels. The image corrupted by quantum noise is shown in Figure 2b. Images restored with the χ^2, independent E and E+RSD constraints are shown in Figures 2c, 2d and 2e, respectively. In the image of Figure 2c only the high spatial frequency components of the noise are removed and the image quality is nearly the same as the original degraded image Figure 2b. When the E constraint

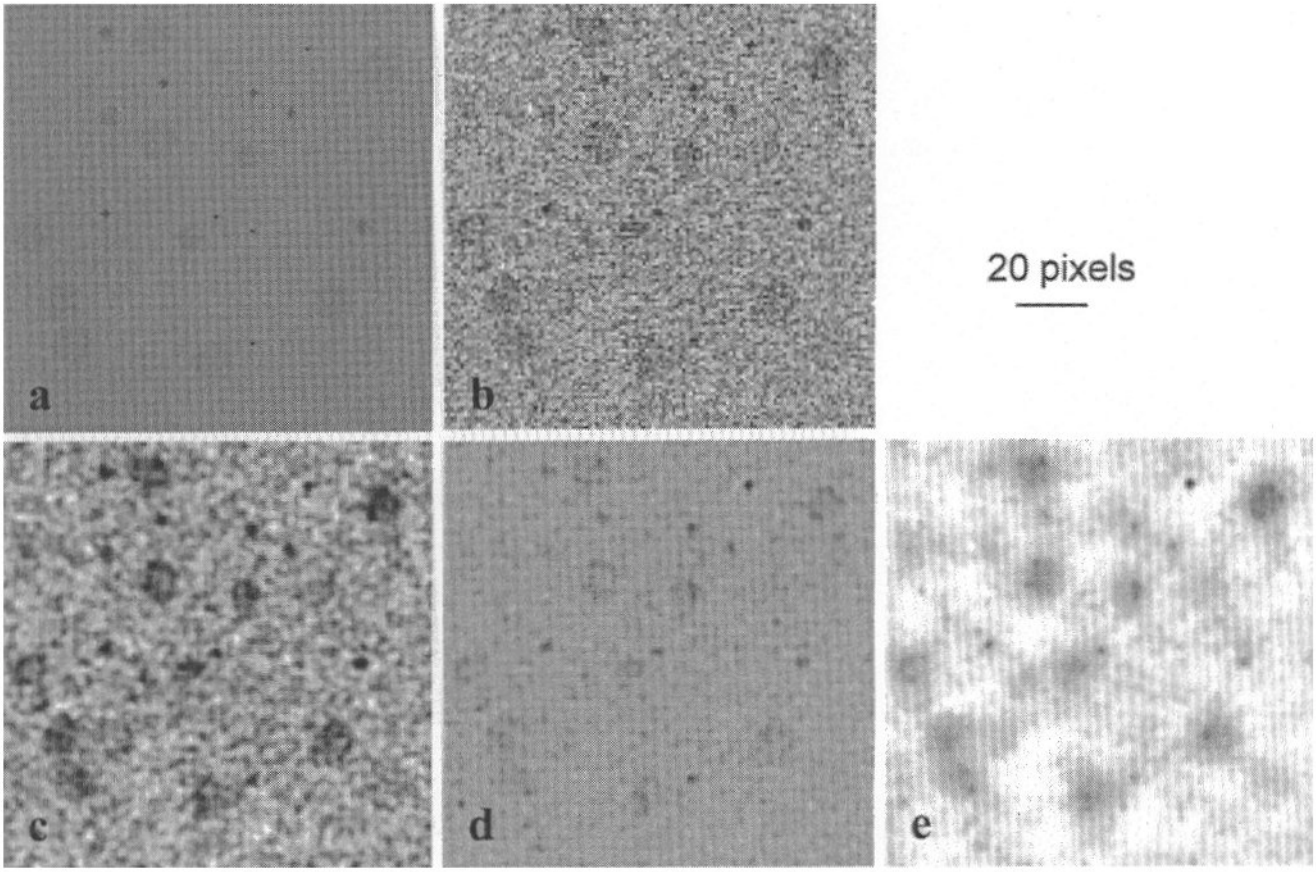

Figure 5. A model of mixed point and disk objects with up to 6 pixels in radius (**a**), its degraded STEM image (**b**) and results of (**c**) χ^2, (**d**) independent E and (**e**) E+RSD constrained ME restorations.

is used independently, the disks completely disappear, as shown in Figure 2d. In the image of Figure 2e restored with E+RSD constraint, the noise is reduced so that the disks are clearly visible. In ME restorations the image without blurring and noise is inferred, that is, the restored image is automatically deconvoluted. In the image of Figure 2e, however, the blurring is not removed. This loss of high spatial frequency components is due to the low SNR of the original image of Figure 2b. The effect of the RSD constraint on the spatial noise distribution is shown in Figure 3 as maps of the residuals $\boldsymbol{n}$. Figure 3a shows the original computer-generated random noise. The maps in Figures 3b and 3c show the residuals inferred by ME restorations with the χ^2 and E+RSD constraints, respectively. In the map in Figure 3b, large negative residuals are localized in the disks. The localization of noise is still recognized in the map in Figure 3c but the degree of the concentration is lower than in Figure 3b. This result indicates that RSD constraint is effective to make the spatial distribution of noise more random and to recover the extended disk objects.

For quantitative evaluation of the effect of restoration, the SNR of the image defined by Rose (1948), which is often used as a measure of visibility, was measured for various disk radii. The measured SNR values are plotted in Figure 4 as a function of the radius of the disk objects. The zero disk radius indicates the point object. The χ^2 constrained ME method could not find the solution for the disk radii of more than 6 pixels and, for smaller objects, presented only a little increase of SNR. The E+RSD constrained ME method yielded SNR higher than the original degraded image for large disks as well as for point objects. Although the restoration with the independent E constraint provides the highest SNR for point objects, it is rejected in the following section because of its ill dependence on the object size.

When many objects with the same configuration exist in an image, as is the case in above model, superposition of images or similar techniques could enhance the SNR of the image. For images containing objects of various sizes, however, these enhancement techniques are not useful. An example of such a case is the model shown in Figure 5a. This model contains point objects and disk objects with

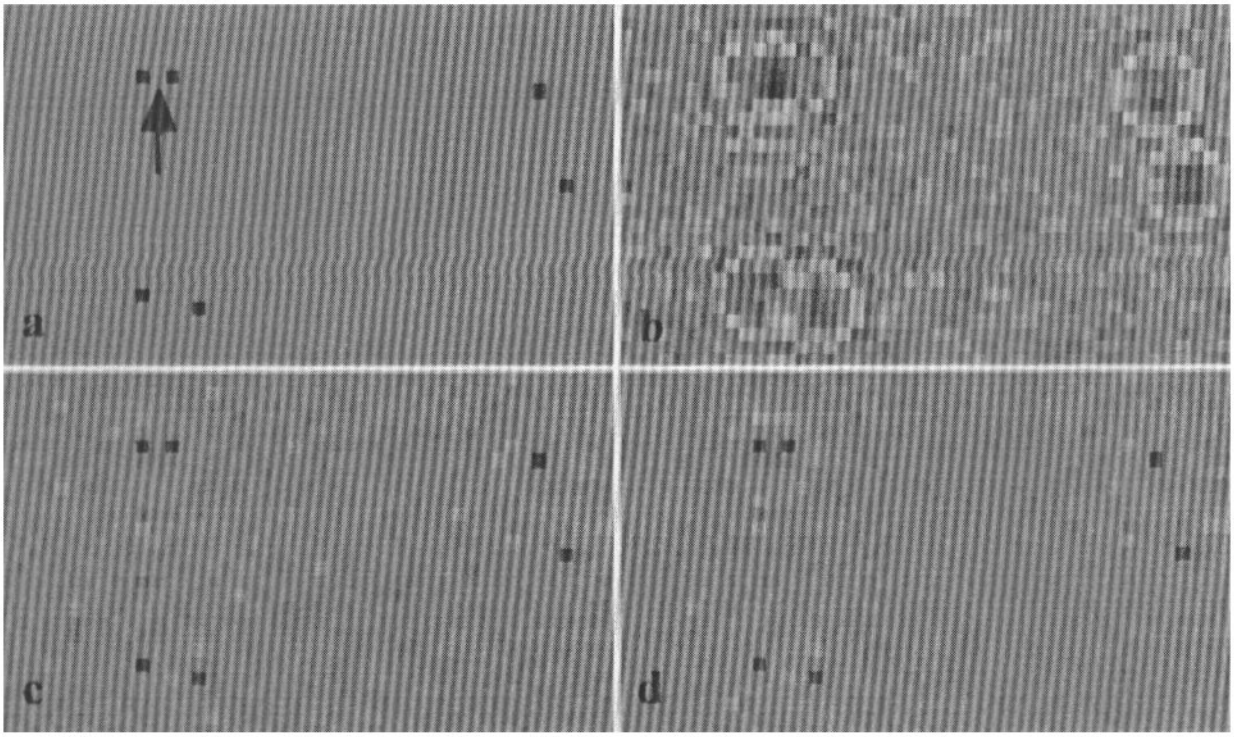

Figure 6. A model of weak-phase point objects (**a**), the defocused TEM image with noise (**b**) and the results of (**c**) χ^2 and (**d**) E+RSD constrained ME restorations. The arrow in (a) indicates a pair of objects separated by one pixel.

various radii up to 6 pixels. The degraded image is shown in Figure 5b. In this image all objects with different radii are imaged with the same SNR of 5 which is the minimum value of the SNR, based on Rose's criterion, required to recognize an object. This means that the averaged intensity in a object measured from the background intensity is inversely proportional to the area of the object. The restored images with the χ^2, independent E, and E+RSD constraints are shown in Figures 5c, 5d and 5e, respectively. The χ^2 constrained ME restoration shown in Figure 5c again failed to decrease the low frequency components of the noise. In Figure 5d, point objects and small disks are observed with high contrasts but large disks are recognized as gatherings of small objects. In Figure 5e, the noise is much reduced and almost all objects with different sizes are simultaneously recovered. This result indicates a practical advantage of the E+RSD constrained ME restoration which can reduce the noise without changing the configurations of objects with various sizes.

Restoration of Models of TEM Images

Effects of the χ^2 and E+RSD constrained ME restorations on TEM images were investigated using model images of weak phase objects. We mainly deal with low resolution images because the low resolution images often contain various structures with different sizes and the E+RSD constrained ME restoration is expected to have the advantage for such images. Radiation-sensitive biological specimens or organic materials are within the scope in this case. Effects of the ME restoration on high resolution images will be described only briefly.

We first consider the low resolution case and, therefore, neglect spherical aberration. Attenuation of the contrast transfer function (CTF) due to chromatic aberration and partial coherence is not taken into account. In this case, the formula of the CTF is written as

$$B(q^*) = 2 \sin (\pi \Delta z^* q^{*2}) \tag{16}$$

with a dimension-less form of spatial frequency and defocus given by

$$q^* = \frac{q}{q_s}, \ \Delta z^* = \Delta z \lambda (q_s)^2 \tag{17}$$

where q denotes the spatial frequency, λ the electron wavelength, Δz the defocus and q_s the sampling spatial frequency (the inverse of the size of a pixel). The shape of CTF depends only on the normalized defocus Δz^*.

An example of the model of randomly distributed

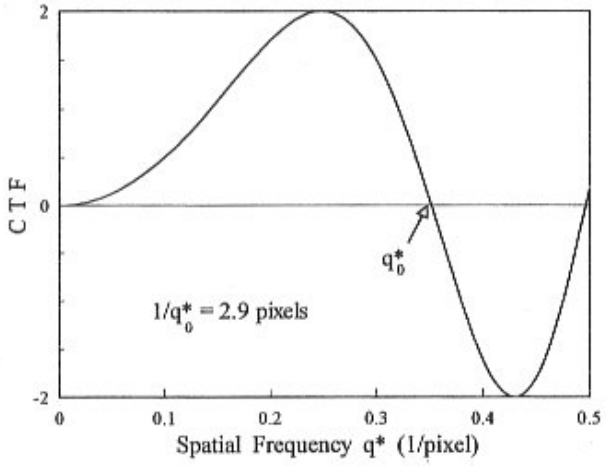

Figure 7. The contrast transfer function used to make the defocused image shown in Figure 6b.

point objects is shown in Figure 6a. A small part of the model with 128x128 pixels is shown to see details of one pixel size. A largely defocused image is shown in Figure 6b for $\Delta z^* = 8.4$. The corresponding CTF is shown in Figure 7. This CTF has two zeros and takes small values near the highest frequency. The image in Figure 7b is corrupted by the Poisson noise whose standard deviation is three times smaller than the peak depth at the objects in the model of Figure 7a before defocusing. In Figure 7b, fringes caused by the defocus are observed around the blurred objects. The results of the χ^2 and E+RSD constrained ME restoration are shown in Figures 6c and 6d, respectively. In these restored images, a pair of points placed at a distance of 2 pixels, shown by the arrow in Figure 6a, are resolved and the noise is obviously reduced. The magnitude of the noise remaining around the objects is almost the same for Figures 6c and 6d. Thus, for point objects, the conventional χ^2 and E+RSD constraints similarly yield deconvoluted images with reduced noise.

Since it is difficult, in practice, to estimate the defocus amount accurately, the effect of the error in defocus estimation was studied for the E+RSD constrained ME restoration. Figures 8a and 8b show the images restored from the image shown in Figure 6b with defocus amounts having 10 and 15 % relative errors, respectively. Figure 8a has almost the same quality as the image in Figure 6c restored with the correct defocus. In Figure 8b, the close two points are not resolved and the background noise becomes larger. From these images the ratio of the contrast to the noise magnitude was measured. The contrast ΔI was defined as the difference between the peak intensity at the restored image of the pair of objects shown by the arrow in Figure 6a and the intensity at their middle pixel. The values of the

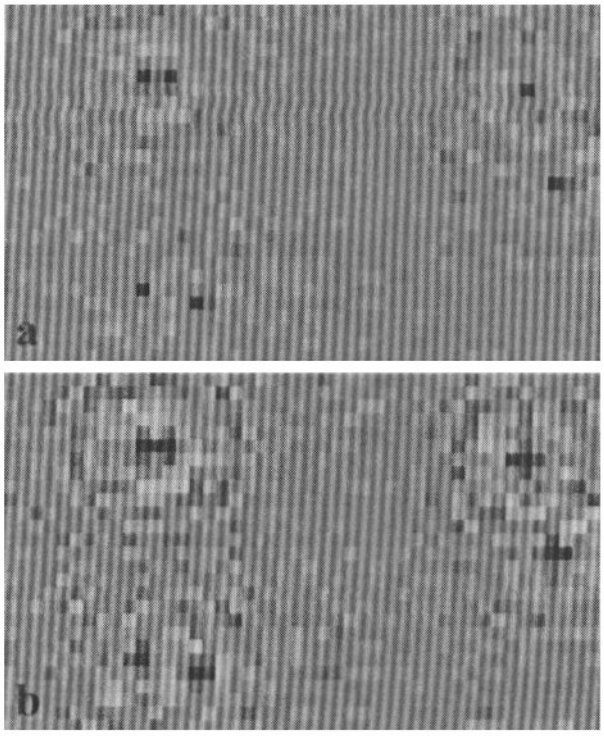

Figure 8. Effects of the error in the estimated defocus amount on the restored image. The relative errors are 10 % for (**a**) and 15 % for (**b**).

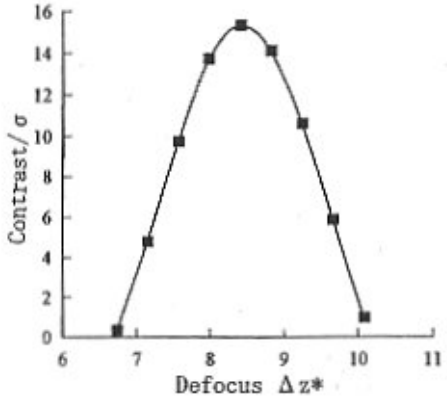

Figure 9. Contrast ΔI of the point objects separated by one pixel, divided by the standard deviation of the background noise σ, plotted as a function of defocus Δz^* used for the restoration. The correct value of Δz^* is 8.4.

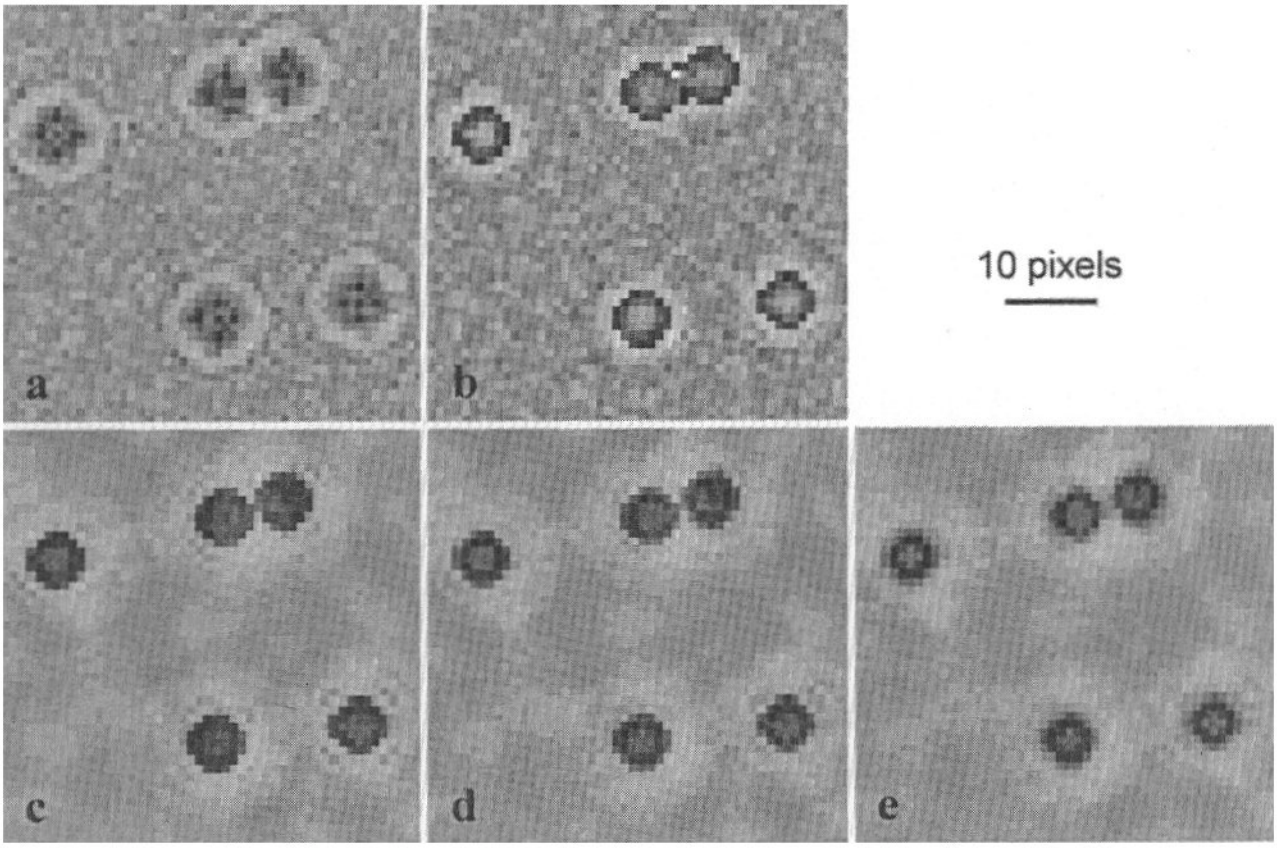

Figure 10. A model of defocused TEM image of weak-phase disk objects (**a**) and the results of the restoration with (**b**) χ^2 and (**c**) E+RSD constraints. Images (**d**) and (**e**) show the effect of the error in defocus amount of 15 % and 30 %, respectively.

ratio $\Delta I/\sigma$, where σ is the standard deviation of the noise in the restored image, are plotted in Figure 9 as a function of the defocus value used for the restoration. The ratio rapidly decreases as the defocus deviates from the correct value of $\Delta z^* = 8.4$ and becomes half at the error of ±13 %. This result indicates that an accuracy higher than 10 % would be required in measurements of defocus amounts to resolve point objects in the restoration of noisy images.

ME restoration of images of extended objects was performed using a model consisting of disks of 6 pixels in diameter. Figure 10a is the image deteriorated with the CTF shown in Figure 7. Figures 10b and 10c are the results of ME restorations with the χ^2 and E+RSD constraints, respectively. In Figure 10b, the fringes due to the defocus are still observed near the edge of disks and the noise level is almost the same as the original image of Figure 10a. In Figure 10c, the contrast of the fringes is much weaker than in Figure 10b and the noise is reduced to small fluctuation of the background intensity with low spatial frequencies. The effect of the error in defocus estimation is shown in Figures 10d and 10e. The error is 15 % for Figure 10d and 30 % for Figure 10e. The appearance of the whole image is not so much changed but the edge of disks is considerably blurred in Figure 10e. The blurring of each point as shown in Figure 8b is canceled in the disks and appears near the edge. This result indicates that the tolerance in the defocus measurements is determined by the visibility of details and not by the total appearance.

Effects of the E+RSD constrained ME restoration on high resolution TEM images were studied with a model image of point objects. Spherical aberration was taken into account and Scherzer focus $\Delta z = \sqrt{C_s \lambda}$ was assumed, where C_s is the spherical aberration coefficient. The cut-off spatial frequency was set to be two times as large as the first zero of the CTF. This means that the length of one pixel is four times smaller than the value of the resolution limit given by $d = 0.71 C_S^{1/4} \lambda^{3/4}$. The corresponding CTF is shown in Figure 11. This CTF has the first zero corresponding to the resolution limit at the spatial frequency of $q_0^* = ¼$ pixel^{-1} and 23 zeros in the region between q_0^* and the maximum spatial frequency of $q^* = ½$ pixel^{-1}. Figure 12a shows the model of point objects convoluted with the CTF shown in Figure 11 and corrupted by noise. The results of the χ^2 and E+RSD constrained ME restorations are shown in Figures 12b and

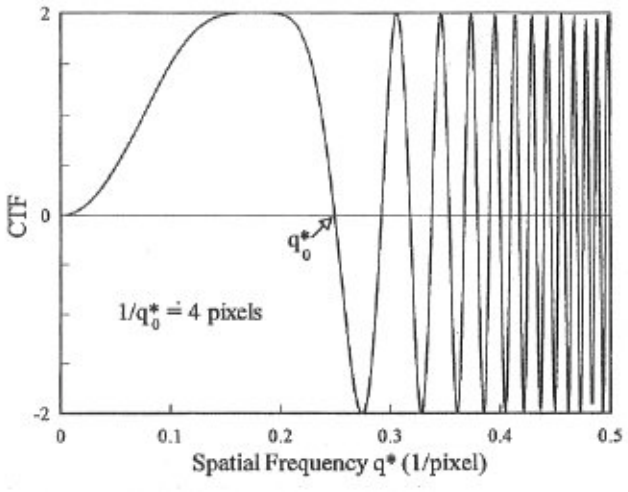

Figure 11. The contrast transfer function at the Scherzer focus. The cut-off spatial frequency is two times higher than the resolution limit.

12c, respectively. In these restored images, the two points at the distance of 2 pixels are resolved and the magnitude of the noise is reduced by a factor of about 6. This result suggests that the ME restoration could improve the resolution by recovering spatial frequency components from the severely oscillating region of the CTF. Actually, attenuation of the CTF due to chromatic aberration and partial coherence would limit the performance of the ME restoration. The effect of the ME restoration on periodic structures, instead of the weak phase objects considered in this paper, must be studied for application to high resolution TEM images.

Conclusion

An improved ME method with a constraint on spatial distribution of noise was proposed as the E+RSD constrained ME method to restore the images of extended objects. The aim of the proposed constraint is to achieve a spatially random distribution of the inferred noise by flattening the power spectrum of the noise. A simple algorithm was developed to realize an approximately uniform power spectrum by fitting the integrated power spectra passed through several low-pass filters to their expectations.

The effects of the E+RSD constrained ME restoration were studied for models of STEM and TEM images numerically. In the STEM case, the image of disk-shaped objects, which was hardly restored with the conventional χ^2 constrained ME restoration, was improved in its SNR. In the maps of the inferred noise residuals, the spatial distribution of the noise amplitude was more random for the E+RSD constrained restoration. From images of point

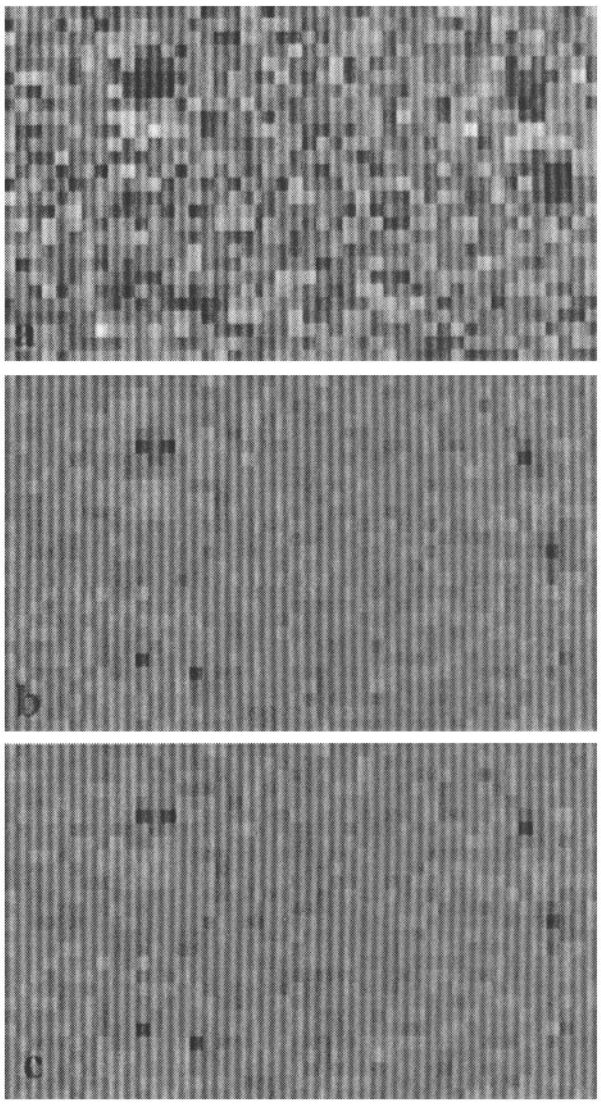

Figure 12. A model of high resolution image at the Scherzer focus (**a**) and the results of (**b**) χ^2 and (**c**) E+RSD constrained ME restorations.

objects mixed with disk objects, the point objects were restored with high contrasts and the noise was fairly reduced. This result indicates the possibility of restoration of fine structures without loss of information on extended objects.

The ME restoration was also applied to models of defocused TEM images. The image of point objects transferred by an oscillating CTF was restored in spite of the existence of zeros in the CTF. It was found that this level of the restoration is possible if the defocus amount is estimated within ±10 % error. For the image of extended objects, the χ^2 constrained ME method was again insufficient both in deconvolution and in noise reduction.

With the E+RSD constrained ME method, the intensity of the fringe due to the defocus became weak and the noise was reduced.

These results of the simulation suggest that the introduction of the constraint on spatial distribution of the inferred noise is effective to restore objects of various size from only one image. This technique, therefore, would be appropriate for observation of radiation-sensitive objects containing a wide range of structure size.

A preliminary simulation was performed for high resolution TEM images. A high resolution beyond the Scherzer resolution limit was obtained from a CTF which has a rapid oscillation caused by spherical aberration. Since the simple weak phase approximation was used in this paper, the effect of the ME restoration on crystalline objects is not clear in the present stage of the development of the improved ME restoration.

Acknowledgments

The work was partly supported by a Grant-in-Aid for Scientific Research from the Ministry of Education, Science and Culture of Japan.

References

Bryan RK, Skilling J (1980) Deconvolution by maximum entropy, as illustrated by application to the jet of M87. Mon Not R Astr Soc **191**: 69-79.

Farrow NA, Ottensmeyer FP (1989) Maximum entropy methods and dark field microscopy images. Ultramicroscopy **31**: 275-283.

Frieden BR (1983) Unified theory for estimating frequency-of-occurrence laws and optical objects. J Opt Soc Am **73**: 927-938.

Gull SF, Skilling J (1984) Maximum entropy method in image processing. IEE Proceedings **131F**: 646-659.

Hanai T, Morinaga, T, Hattori A, Hibino M (1994) Improvement of maximum entropy method for reduction of the statistical noise in electron microscope images. Electron Microscopy 1994 **1**: 435-436.

Hu JJ, Li FH (1991) Maximum entropy image deconvolution in high resolution electron microscopy. Ultramicroscopy **35**: 339-350.

Kikuchi R, Soffer BH (1977) Maximum entropy image restoration. I. The entropy expression. J Opt Soc Am **67**: 1656-1665.

Narayan R, Nityananda R (1986) Maximum entropy image restoration in astronomy. Ann Rev Astron Astrophys **24**: 127-170.

Pennycook SJ, McGibbon AJ, McGibbon MM, Browning ND, Chisholm MF, Jesson DE (1994) Determination of interface structure and bonding at atomic resolution in the STEM. Electron Microscopy 1994 **1**: 345-348

Rose A (1948) Television pickup tubes and the problem of vision. Adv Electronics Electron Physics **1**: 131-165.

Skilling J, Bryan RK (1984) Maximum entropy image reconstruction: general algorithm. Mon Not R Astr Soc **211**: 111-124.

Discussion with Reviewers

P.W. Hawkes: The ME method is particularly well suited to images with reasonably marked features, preferably separated by fairly uniform zones (diffraction patterns for example). Do the authors consider that their procedure would still be beneficial for electron images full of high-resolution details?

Authors: Yes, we expect the ME method could be applicable to high-resolution images. It is true that the method is suited to images with marked peaks on a uniform background and not to complicated structures with irregular intensity distributions. But we consider the weakness of the ME method could be overcome by an appropriate estimation of the spatial distribution of noise. A proposal for this purpose was described in this paper. The difficulty would arise in determining accurate imaging parameters as other restoration methods using only one image. From this point of view, methods using though-focus series would be better if the specimen is not sensitive to electron irradiation.

P.D. Nellist: The authors have used two low-pass filters plus the total power of the noise residual to provide the spatial distribution constraint. How have the authors chosen the number of low-pass filters to use? Is there a criterion for the optimal number of filters to use for a given accuracy?

M. Op de Beeck: For simplicity only two low pass filters are assumed in the paper. How do the reconstructions depends on the number of low pass filters and on the shape?

Authors: It would be better, at least mathematically, to fit each spatial frequency component to a uniform power spectrum independently. But this is very time-consuming and practically impossible. Therefore, we decreased fitting parameter by using integrated powers. Besides, we divided low frequency region into smaller pieces than high frequency region because the noise concentrated on extended objects is considered to make the power spectrum irregular especially in the low frequency region. The number of the filter was increased until the change of the appearance of the processed image was not recognized, and typically 6-10 filters were used. Other shapes of the filter is not tried to use yet.

M. Op de Beeck: The performance of the RSD+E constraint

has been demonstrated on images with low signal to noise ratios. Would the method show the same improvement over the existing ME method in case of high SNR?
Authors: No, the degree of improvement would be lowered for high SNR images because the localization of large noise would not so much affect the visibility of the image if the noise amplitude is sufficiently small. The deconvolution effect of the E+RSD constrained ME method is almost the same as that of the existing ME method.

M. Op de Beeck: The RSD+E method inherently favourises low frequencies in the reconstructed images by simultaneously maximizing the entropy in different resolution ranges. Would a weighted E-constraint optimization yield comparable results?
Authors: No, we do not think so. ME restorations usually enhance high spatial frequencies by increasing the height of marked peaks and decreasing small fluctuations to maximize the entropy. The noise is assigned to produce such an image. This is a fundamental property of ME methods including a weighted E-constraint, in which only the probability distribution is constrained to fit the real noise. Constraints on the spatial distribution operates to assign the noise equally to the marked peak and the background, and result in the recovery of low frequencies.

E.J. Kirkland: The maximum entropy method obtains much of its advantage because it enforces a "positivity" constraint on the image and reduces spurious negative oscillations (i.e., Gibbs oscillation). This requires knowledge of real background constant in the image. Practical measured images typically have an arbitrary linear scaling factor and offset. Can you comment on the practical requirements of using the maximum entripy method on real measured images?
Authors: The positivity constraint on the intensity is not so important in our method because we do not use the background subtraction used in usual ME methods and the model images have high background. But knowledge of the background level is still required to estimate the magnitude of the noise because we suppose the Poisson noise whose amplitude is identical to the square root of the electron number. In application to real electron images, we have to also consider the noise generated in the detection and recording system used. Since it is difficult to measure the fluctuation of electron number and the noise of the recording system separately, it would be better to measure SNR of image recorded for a uniform illumination without specimen and take the square of the SNR as the effective electron number which is used to represent images in the ME restoration program. Calibration of the detection and recording system with respect to the number of incident electrons would be also necessary to avoid non-linearity and offset of recorded images.

E.J. Kirkland: What are the accuracy requirements for the other relevant parameters such as magnification and spherical aberration C_s? Do you expect STEM to be more or less sensitive to the accuracy of image parameters than TEM?
Authors: Errors in estimating magnification and spherical aberration result in a shift of contrast transfer function which causes reversal of the sign of the CTF in some spatial frequency ranges. The effect of the errors would be sever when the CTF oscillates rapidly in the high frequency region. This is one of reasons why we concentrate on noise reduction in low resolution images for which the CTF oscillates gently and, therefore, the accuracy requirements for the imaging parameters are relatively low. We expect STEM to be less sensitive to the accuracy because the incoherent nature of the STEM imaging suppresses the contrast reversal. Measurements of Gaussian probe size are easier than measurements of the spherical aberration coefficient and the absolute defocus amount.

E.J. Kirkland: Do you expect the defocus accuracy requirements to be different for different choices of defocus?
Authors: Yes, the accuracy requirements would be higher for larger defocus in the case of low resolution images because the oscillation of the CTF becomes more rapid. In the case of high resolution images, we expect that there is the optimum defocus which relaxes the oscillation of the CTF in high spatial frequency region.